ELSEVIER

26 December 1994

PHYSICS LETTERS A

Physics Letters A 196 (1994) 173–180

Transient chaos as the backbone of dynamics on strange attractors beyond crisis

K.G. Szabó, T. Tél

Institute for Theoretical Physics, Eötvös University Budapest, Puskin u. 5–7, Budapest H-1088, Hungary

Received 25 March 1994; revised manuscript received 8 August 1994; accepted for publication 1 November 1994
Communicated by A.P. Fordy

Abstract

We show that chaotic attractors at and above internal crisis points can be naturally decomposed into nonattracting invariant chaotic sets connected by weak intermittent heteroclinic couplings. These basic component sets are used to obtain the dynamical multifractal spectrum characterising the asymptotic and the finite time dynamics on the entire attractor.

1. Introduction

Transient chaos has been analysed extensively as a behaviour preceding the motion on a (simple or chaotic) attractor (for a review see Ref. [1]). In such cases, there exists a nonattracting invariant set in the phase space along with the attractor. The nonattracting invariant set is typically a chaotic saddle which is globally repelling but has nevertheless a basin of attraction of measure zero. In strongly dissipative systems characterised by one-dimensional maps it degenerates to a repeller with a Cantor-set-like structure.

In this paper, we would like to point out that transient chaos provides a useful characterisation of the *permanent* chaotic motion on chaotic attractors as well.

In particular, we show that in certain situations there is a natural way to decompose a chaotic attractor into nonattracting chaotic sets (either chaotic saddles or repellers) that are weakly coupled and play a determining role in the motion on the attractor. We call them hereafter the *basic nonattracting components* of the attractor. This is the case with chaotic attractors beyond internal crises [2] a situation well accessible in experiments [3–5]. The importance of nonattracting chaotic sets at crisis or in the precritical region has been mentioned in a few previous publications [4,6–9] from the point of view of different multifractal spectra. Our results complete this picture by emphasising that the *postcritical* chaotic attractor can be decomposed into nonattracting invariant subsets. These basic components exhibit fractal structure along the unstable foliation, providing thus a *geometrical backbone* of the attractor. We give an explicit procedure for the construction of these components.

Although generating transient chaos, the basic components also provide a *dynamical backbone* of the asymptotic motion, in the sense that their dynamical multifractal spectra yield a good approximation of the dynamical characteristics of the whole attractor.

The basic components are dynamically coupled via heteroclinic orbits. They develop from a single heteroclinic orbit appearing at crisis that is of marginal stability, and form a new component of the dynamics. This component contains an infinite number of very long periodic orbits whose stability might be close to

SSDI 0375-9601(94)00898-1

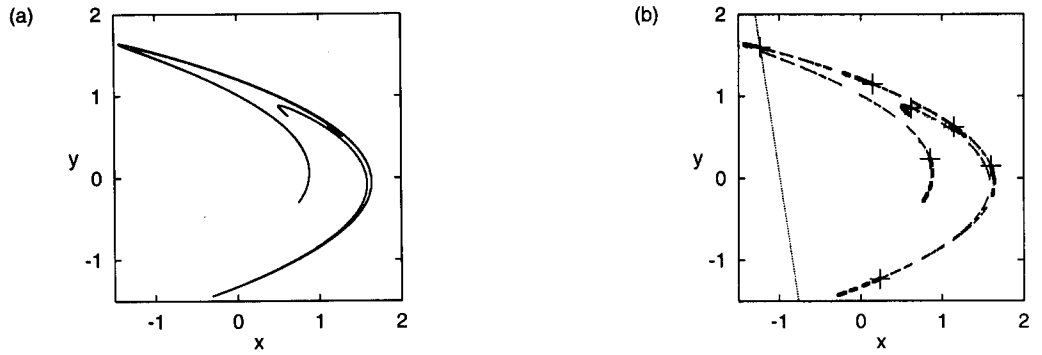

Fig. 1. The attractor of the Hénon map $(x, y) \mapsto (a - x^2 + by, x)$ (a) and the two chaotic saddles (b), the *basic components*, forming the backbone of the dynamics on the attractor. The parameters are $b = 0.3$ and $a = 1.276$ taken in the postcritical regime *above* a period-7 window (the crisis value is $a_c = 1.2716856$). The component which is invariant under the seven-fold iterated map (heavy dots) is located in seven bands. The invariant subset restricted to the complement of these bands forms the other basic component (light dots). Both chaotic saddles exhibit a pronounced fractal structure along their unstable manifolds. The period-7 orbit (+) *mediates* between the two basic components. The first component was plotted by selecting pieces from a single trajectory on the attractor, while for the second 10000 evenly distributed trajectories were started from the interval $|x| \leqslant 0.5$, $y = 0$. In both cases the dotted straight line, which is tangent to the local stable manifold at the leftmost mediating periodic point and does not intersect other parts of the attractor, was used to identify numerically the points falling into the leftmost band of the first component, as described in the text.

marginal. The dynamics associated with this component can only be seen in long-time observations. Then the associated orbits form the "bulk" of the postcritical chaotic attractor as they fill in the gaps along the unstable foliation of the basic nonattracting components.

Because of the separation of time scales in the postcritical region, we can distinguish the finite time characteristics of the system from the truly asymptotic ones. The asymptotic dynamical spectrum of the entire attractor can be approximately obtained as the convex hull of the contributions of the basic components and of the heteroclinic connection, while the finite time behaviour is faithfully characterised by superimposing the spectra of the basic components only. These properties approximately hold in the postcritical regime, even for parameter values considerably far above the crisis point.

2. Constructing the basic components

Crisis itself is the tangency of the attractor with the stable manifold of a *mediating periodic orbit* [2]. This stable manifold acts as the boundary of the basin of attraction of the precritical attractor separating it from other invariant sets. The very same manifold provides a natural partitioning of the *post*critical chaotic attractor; this fact can be used to construct the basic components.

Suppose that the mediating orbit is an m-cycle. The local pieces of the stable manifold of the period-m orbit divide the attractor into bands. The subset of the attractor that is invariant under the m-fold iterated map is located, in general, in m bands. It forms one of the basic nonattracting components. The invariant subset within the complement of these bands forms another basic component.

Numerically one can obtain these sets by following a very long chaotic trajectory on the whole attractor and selecting segments that for many iterations either return on each mth step to a given band or never enter this band at all. The two sets can be plotted after discarding the last few points of these segments, as usual in case of transient chaos [10,1]. Alternatively, the PIM-triple method [11] (with the same selection criterion) can also be used to determine the basic components.

As an example, Fig. 1 shows the attractor of the Hénon map in the postrictical regime above a period-7 window and its decomposition into basic components, namely two chaotic saddles.

The crisis illustrated with the Hénon example is a case of *attractor explosion* [7,9,12–21]. *Attractor merging* [2,6,22,23] is a related phenomenon when two or more disjoint coexisting attractors become parts

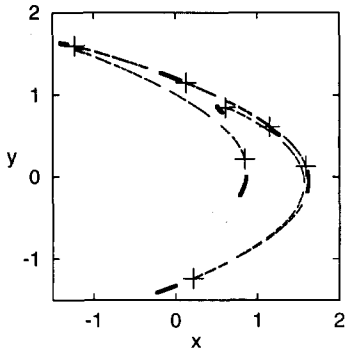

Fig. 2. The invariant sets of the Hénon map in the precritical regime, *inside* the period-7 window, at $b = 0.3$ and $a = 1.266$. A chaotic saddle (light dots) coexists with the seven-piece chaotic attractor (heavy dots). The would-be mediating period-7 orbit (+) is on the edge of the saddle. When reaching the crisis value $a_c = 1.2716856$, the attractor collides with the saddle at this orbit. Beyond crisis the remnant of the seven-piece attractor and the continuation of the precritical saddle become the two basic component saddles shown in Fig. 1b. The precritical saddle was plotted the same way as in the postcritical case in Fig. 1.

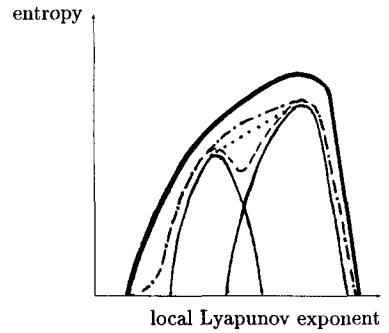

Fig. 3. A qualitative picture demonstrating how the basic components determine the multifractal spectra of the system in different measurements. The horizontal axis is a local Lyapunov exponent, the vertical, some entropy. The solid lines show the multifractal spectra of the individual basic components if measured separately, the thick line, that of the whole chaotic set. The dashed and dash-dotted lines show the anticipated outcomes of short-time measurements when the entropy is obtained directly or via the partition sum: they are expected to run close to the maximum or the convex hull (dots) of the basic components' spectra, respectively. The small difference comes from the negligible contribution from the heteroclinic coupling component.

of an enlarged attractor. The situation is then very similar to that of attractor explosion, except that in this case there are more than one precritical attractors. If the system has certain symmetries, internal crisis might also occur in the form of symmetry recovering attractor merging [22].

We note that the basic components are the continuation of the attracting and nonattracting sets that exist before the crisis: the precritical attractor (which may well consist of several pieces) and a coexisting nonattracting set. In the case of the Hénon map these precritical sets are shown in Fig. 2.

3. The entropy functions of composed attractors

There have been different entropy-like functions introduced for the characterisation of the dynamical multifractal behaviour. They are connected with the statistics of trajectories with a given local property. Notable examples are the $g(\Lambda)$ [24] and the $\phi(\lambda)$ [25] functions based on the path probabilities and the finite time Lyapunov exponents, respectively. Alternatively, they can also be obtained as Legendre transforms of certain free energy like quantities (e.g., the Rényi entropies in the case of $g(\Lambda)$) extracted from appropriate partition sums (cf. Section 4). In the next section a third, less often used, but for our purposes rather convenient entropy function, $S(E)$, will be discussed. The graph of all of these functions is convex and the analysis of the dynamics on composed attractors proceeds along the same lines for all of them. Therefore, in this section we shall not specify the particular form, we shall just speak of an abstract entropy as a function of a kind of local Lyapunov exponent. Each basic component possesses its own entropy function supported on a finite interval (for a schematic diagram, see Fig. 3). These intervals might partially overlap indicating that the same value of local Lyapunov exponents can occur in different basic components.

The entropy functions of the basic components are, of course, smaller than the entropy of the whole attractor (thick line in Fig. 3). The difference between the attractor's and the basic components' entropy comes from the contribution of the third, heteroclinic coupling component. It is hard to say anything in general about this latter contribution, however, we can certainly say that somewhat above crisis there are coupling orbits close to marginality, i.e. with small local Lyapunov exponents. A considerable amount of entropy may belong to these orbits, therefore we expect that the entropy difference between the attractor and

the basic components is significant on the left hand side, and it is always present in this region.

The entropy function of the whole attractor thus builds up from the contributions discussed above. In case of an *actual observation*, however, its form depends on the time scale and the way of the measurement. Let us denote the longest characteristic time scale of the motion on the basic components by τ; close to the crisis this comes from the remnant of the precritical attractor, and is typically much shorter than the minimal length τ' of coupling orbits.

On short time scales, when the observation time T is on the order of τ, the coupling component cannot be observed. Then, a direct analysis of the local Lyapunov exponents yields an entropy function very close to the maximum of the basic components' spectra (dashed line in Fig. 3). When performing a different analysis based on the appropriate partition sum (cf. Section 4), as a consequence of taking a Legendre transform, the resulting entropy function (dash-dotted line) will appear close to the convex hull of the basic components' entropy contribution.

In the case of asymptotically long-time analyses, $T \approx \tau'$, a direct determination of the statistics of trajectories with a given local Lyapunov exponent is hopeless, thus one has to use a partition sum approach and obtain the entropy via Legendre transformation. Such a measurement will yield the entropy function of the attractor (thick line in Fig. 3). Due to the extra contribution of the coupling orbits, which is pronounced on the left hand side, it runs somewhat above the convex hull of the basic nonattracting components' entropy.

On intermediate time scales $\tau \ll T \ll \tau'$, the measured entropy function only gradually exceeds the shape determined by the basic components (whichever method is used). Thus the backbone remains a good approximant for the entropy of the attractor even on such time scales.

4. The geometrical multifractal spectrum

We propose the use of the so-called geometrical multifractal entropy function $S(E)$ [26,27], since it seems to be particularly useful in describing the essence of the phenomenon. Here the number of trajectories is investigated rather than their probability taken with respect to the natural measure, and this is why we call it a geometrical multifractal characteristic.

In the case of a single invariant set in a two-dimensional map, the entropy function is defined as follows. Cover the set in a generating partition with hierarchically nested "boxes" of linear sizes $\{\epsilon_i\}_{i=1}^{N(n)}$ along their local unstable direction at each level n of the partition. These length scales decrease exponentially in n, thus, local scaling exponents E_i can be introduced via the relation $\epsilon_i = \exp(-E_i n)$ for each "box". Since the nth images of the partitioning boxes extend to the whole set, E_i can be considered as the growth rate of expansion, i.e. the local Lyapunov exponent. As n grows, there is an increasing number $N(n, E)$ of boxes having the same exponent E. This growth is exponential in n again, and the rule $N(n, E) \sim \exp[S(E)n]$ defines the entropy function. Thus, $S(E)$ can be interpreted as the *topological entropy* of trajectories with local Lyapunov exponent E.

Alternatively, S can be extracted from a partition sum Z_S and the associated free energy $F(\beta)$ defined as

$$Z_S = \sum_{i=1}^{N(n)} \epsilon_i^{\beta} \sim \exp\left[-\beta F(\beta) n\right] \tag{1}$$

by taking the Legendre transform of $\beta F(\beta)$. For comparison it is worth also giving the partition sums connected with the other two entropy functions mentioned in the previous sections,

$$Z_g = \sum_i P_i^{\beta}, \tag{2}$$

and

$$Z_\phi = \sum_i P_i \epsilon_i^{-\beta}. \tag{3}$$

Both of them incorporate metric properties connected with the natural measure P_i of the "boxes", in contrast to the purely geometric definition of (1).

The graph of $S(E)$ must be a single humped convex function whose maximum is the topological entropy of the set, and the E value where the graph has a unit slope can be shown [26] to be the average Lyapunov exponent. For attractors, the $S(E)$ curve touches the diagonal $S = E$ while, for nonattracting sets, $S(E)$ is shifted to the right by the amount of its escape rate κ.

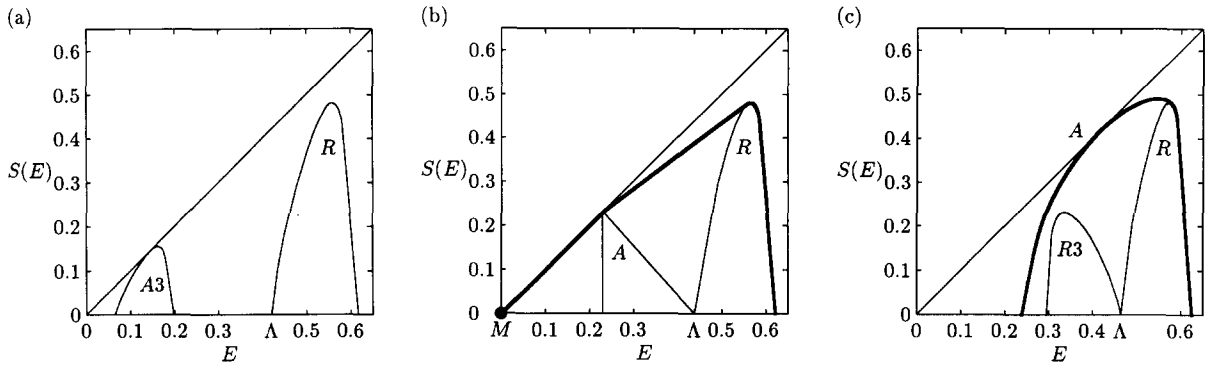

Fig. 4. Entropy spectra of the quadratic map $x \mapsto 1 - ax^2$ around the attractor explosion at the end of the period-3 window. The entropies were obtained by the constrained Frobenius–Perron operator method as it has been worked out in Ref. [29]. The Lyapunov exponent of the mediating period-3 orbit is denoted by Λ. In the precritical region (a), at $a = 1.785$, the three-piece attractor ($A3$) and the coexisting repeller (R) have disjoint entropy spectra. At the crisis value $a = a_c = 1.7903275$ (b), besides these, a marginally stable heteroclinic orbit yields the third component (M) in the origin. Then the asymptotically exact entropy of the entire system (A) is given by the convex hull (solid line) of the three components. In the postcritical region (c) the remnant of $A3$ becomes a three-piece repeller, $R3$, while its entropy spectrum is shifted to the right, below the diagonal. The other basic component remains practically unchanged. These spectra reflect short lifetime behaviours of the two intermittent chaotic phases. The entropy of the entire attractor (A) describing the asymptotic dynamics is somewhat over the convex hull of the two repellers.

We briefly sketch a method that can be applied to invertible two-dimensional maps. The basic nonattracting sets can be constructed, as discussed in Section 2, (cf. Fig. 1b) by computing a few branches of the mediating orbit's stable manifold, thus specifying regions containing the sets. In order to find the entropy function one can use a procedure worked out originally for scattering processes [30]: start trajectories along a line outside of the specified regions and follow how long they remain inside these regions. Increasing lifetimes define intervals arranged in a hierarchical order. Measuring their sizes defines length scales $\{\epsilon_i\}$, very much in the same way as in one-dimensional cases, from which the entropy function can be derived.

However, the most powerful method for determining $S(E)$ has been worked out for one-dimensional maps: it can be obtained from the largest eigenvalue of the generalised Frobenius–Perron operator [28]. By restricting this operator to the basic components (which are repellers in this case) the partial entropy contributions can also be determined [29].

5. Example for the decomposition of the entropy function

In order to gain qualitative verification of the theory outlined above we made exact calculations for determining the entropy spectrum in the quadratic map

$$x \mapsto 1 - ax^2. \tag{4}$$

We have investigated not only the postcritical case but the full vicinity of the attractor explosion point at the end of the period-3 window, which is the one-dimensional analogue of the phenomenon shown in Figs. 1 and 2. In Fig. 4 we demonstrate how the $S(E)$ function changes when the control parameter a passes through the the crisis value $a = a_c = 1.7903275$.

(a) In the precritical region, within the main period-3 window $a \in [1.75, a_c]$ of the map (4), analogously to the situation in Fig. 2, there is a three-piece attractor ($A3$) and, an additional chaotic repeller (R) with a Cantor-set-like structure. These two invariant sets are responsible for the asymptotic behaviour and the preceding chaotic transients of the system, respectively. Fig. 4a shows the free energy functions of the three-piece attractor and the coexisting repeller obtained by using the constrained Frobenius–Perron operator method [29], at $a = 1.785$, a control parameter

value where the attractor is chaotic. Note that the entropy function of the component sets are disjoint. Apparently, the transient behaviour of this system is more chaotic than the asymptotic one because the $S(E)$ spectrum of the repeller is much further away to the right than that of the attractor (i.e., it has strictly larger local Lyapunov exponents) and, also, has a greater maximum (i.e., topological entropy). We note that the local Lyapunov exponent, Λ, of the mediating period-3 orbit is the smallest on the repeller.

(b) At the crisis situation $a = a_c$ the three-piece attractor just touches the repeller at the mediating orbit. Fig. 4b shows that the mediating orbit indeed gives a contribution (at $E = \Lambda$) to the spectra of both basic components. Due to this heteroclinic tangency, an additional coupling component also appears in the system in the form of an infinitely long marginal orbit (M). Since its topological entropy and Lyapunov exponent are both zero, this component can be represented by a single point at $S = E = 0$. Because the coupling is *infinitely weak* at crisis, the resultant entropy function is the mere *superposition* of the entropies of the main components: the old attractor ($A3$), the repeller (R) and the heteroclinic orbit (M). This rule holds as long as finite time observations are made. The asymptotic result, on the other hand, can be obtained as the *convex hull* of the main components' contribution. This implies the appearance of the straight lines connecting the old attractor's entropy contribution to the graphs belonging to the mediating orbit and the nonattracting set, respectively. The piece on the diagonal $S = E$ in the entropy spectrum has previously been described [31] as a general sign of intermittency. (We note in passing that the reason of the triangular shape of the entropy of $A3$ in Fig. 4b is that $A3$ undergoes a phase transition when it collides to the mediating orbit. This situation is the counterpart of the phase transition at the external crisis point $a = 2$ [32] where the attractor practically becomes a two-scale set.)

(c) Beyond the crisis ($a > a_c$) there is only a single, one-piece enlarged attractor (A). Just like in the analogous case shown in Fig. 1b, there are two basic components *embedded* in the attractor. Both of them are repellers now with a Cantor-set-like structure. One of them inherits the topological structure of the precritical repeller, therefore, we keep denoting this subset by R. The other one consists of those orbits that never escape from the three bands of the former attractor $A3$; this set will be called hereafter the three-piece repeller ($R3$).

By considering the $S(E)$ functions at $a = 1.8$, somewhat beyond the crisis situation, in Fig. 4c, it is conspicuous that the spectrum characterising the whole attractor, obtained from an asymptotic measurement, runs somewhat above the common convex envelope of the curves belonging to the two repellers. This fact shows convincingly that the multifractal spectra of the embedded repeller components can indeed be used as a sort of backbone, to approach the spectrum of the whole attractor.

Such an approach provides us with some information on the internal structure of the attractor and on the characteristics of the asymptotic behaviour too; for example the escape rates from the individual basic components determine the average lifetime and typical frequency of bursts characterising crisis induced intermittency [14]. These quantities give the *characteristic time scales* of chaotic transients on the repellers R and $R3$, respectively. In the vicinity of a_c these time scales remain significantly shorter than that of the third, heteroclinic component which is determined by the diverging lengths of the coupling orbits. This makes sure that on time scales of τ, the reciprocal value of the smallest escape rate, one observes just the union of the basic components' entropy contributions rather than the full spectrum, as described in Section 3.

We emphasise that the property of decomposability holds considerably beyond a_c. However, it is difficult to tell in general what the region of validity of the decomposition suggested in this paper is. The relative difference in the control paramater from the crisis value $(a/a_c - 1)$ is not necessarily a proper quantity. It is clear from Fig. 4 that although the relative difference is rather small, the actual shape of the basic components' entropy function undergoes a considerable change. In contrast to previous papers [6,7,9] restricted to an infinitesimal vicinity of the crisis configuration, we claim that by determining the basic components and their entropies at a rather than at a_c, the decomposition suggested might be a good approximation even at such control parameter values where the dynamics on the basic components considerably differs from that at crisis.

In our example the entropy functions of the basic components do not overlap (cf. Figs. 3 and 4): they

only touch each other at A, the local Lyapunov exponent of the mediating orbit all over the postcritical region. This fact is a consequence of the specific map, and this is not necessarily true for other one-dimensional maps and is certainly atypical for higher dimensional systems.

6. Closing remarks

The picture we outlined in this paper is particularly practical to demonstrate the mechanism how the topological entropy and the average Lyapunov exponent changes when the system undergoes a crisis. Fig. 4 shows well that when the enlarged attractor appears, its entropy function takes up the maximum value exactly where the former repellers' spectrum does. Therefore, when the enlargement happens, the topological entropy of the attractor jumps suddenly from the value of the precritical attractor's to that of the precritical repeller. (There is of course no jump in the topological entropy of the whole system.) The Lyapunov exponent of the attractor, i.e. the place where the $S(E)$ function is tangent to the diagonal also departs rapidly (although continuously) to the right from its original, precritical value as the system parameter exceeds the critical value. This is consistent with the observation that the Lyapunov exponent of the postcritical attractor is typically larger than that of the precritical one(s) [15].

An important advantage of our method is that the nonattracting sets selected as basic components are particularly *robust*, in contrast to the attractor which is extensively sensitive to changes in the control parameter, as it was discussed above. In one-dimensional systems the basic components are typically *structurally stable*: their orbits do not appear, disappear nor change stability. In higher dimensions this is not general [33], however, the basic components are much less sensitive than the contribution of the newly appeared connecting orbits.

We would like to recall that the basic nonattracting components, as we defined them in the most natural way, can be associated with the different chaotic phases in crisis induced intermittency [14].

This mechanism has been described in the case of the $\phi(\lambda)$ spectrum [6,7] by assuming the entropy contribution of nonattractive sets inside the attractor without explicitly determining them. In this paper we argue that this phenomenon is general for all kinds of entropies around crises. We show that the basic components can be constructed, and their individual entropy functions can, in fact, be measured.

We also mention that, according to our results, attractor enlargement provides a good example for *multitransient chaos* [20] in the sense that the dynamics of weakly coupled non-attracting chaotic sets can be used successfully to analyse the motion on the joint chaotic attractor.

Acknowledgement

The authors acknowledge illuminating discussions with C. Beck, C. Grebogi, L. Kocarev and Z. Kovács and the useful comments of E. Kostelich. This work has been supported by the Hungarian National Science Foundation (OTKA) grants 2090, T4439, F4286. The research has been carried out partially in the framework of the PHARE ACCORD program H9112-0378.

References

[1] T. Tél, in: Directions in chaos, Vol. 3, ed. Hao Bai-lin (World Scientific, Singapore, 1990) pp. 149–211.
[2] C. Grebogi, E. Ott and J.A. Yorke, Phys. Rev. Lett. 48 (1982) 1507; Physica D 7 (1983) 181.
[3] T.L. Carroll, L.M. Pecora and F.J. Rachford, Phys. Rev. Lett. 59 (1987) 2891;
W.L. Ditto et al., Phys. Rev. Lett. 63 (1989) 923.
[4] R. Stoop and J. Parisi, Phys. Rev. A 43 (1991) 1802.
[5] J.C. Sommerer, W.L. Ditto, C. Grebogi, E. Ott and M.L. Spano, Phys. Lett. A 153 (1991) 105;
J.C. Sommerer, in: Proc. 1st Experimental Chaos Conference, eds. S. Vohra et al. (World Scientific, Singapore, 1992) pp. 269–282; Phys. Lett. A 176 (1993) 85;
M. Franaszek and L. Fronzoni, preprint (1993); in: Proc. 2nd Experimental Chaos Conference, to be published.
[6] T. Horita et al., Prog. Theor. Phys. 80 (1988) 793.
[7] K. Tomita et al., Prog. Theor. Phys. 81 (1989) 1124.
[8] Lj. Kocarev and Z. Tasev, Dimensional characterization of basin boundaries in one-dimensional maps, preprint (1991).
[9] R.W. Leven, M. Selent and D. Uhrlandt, preprint (1993), to appear in Chaos Solitons Fractals.
[10] H. Kantz and P. Grassberger, Physica D 17 (1985) 75.
[11] H. Nusse and Y. Yorke, Physica D 36 (1989) 137.
[12] R.W. Leven and B.P. Koch, Phys. Lett. A 86 (1981) 71.
[13] C. Grebogi, E. Ott and J.A. Yorke, Phys. Rev. Lett. 57 (1986) 1284.

[14] C. Grebogi, E. Ott, F. Romeiras and J.A. Yorke, Phys. Rev. A 36 (1987) 5365.
[15] B. Pompe and R.W. Leven, Phys. Scr. 38 (1988) 651.
[16] K. Tomita et al., Prog. Theor. Phys. 80 (1988) 953.
[17] J.C. Sommerer, E. Ott and C. Grebogi, Phys. Rev. A 43 (1991) 1754.
[18] H. Shibata, H. Fujisaka and H. Mori, Phys. Lett. A 189 (1992) 554.
[19] M. Franaszek and A. Nabaglo, Phys. Lett. A 178 (1993) 85; 182 (1993) 99.
[20] M. Franaszek, Phys. Rev. A 46 (1992) 6340.
[21] Y.-C. Lai, C. Grebogi and J.A. Yorke, in: Applied chaos, eds. J.H. Kim and J. Stringer (Wiley, New York, 1992) pp. 441–456.
[22] H. Fujisaka, H. Kamifukumoto and M. Inoue, Prog. Theor. Phys. 69 (1993) 333;
F.T. Arecchi, R. Badii and A. Politi, Phys. Lett. A 103 (1984) 3;
K. Aoki, O. Ikezawa and H. Kamifukumoto, Phys. Lett. 106 A (1984) 343;
H. Ishii, H. Fujisaka and M. Inoue, Phys. Lett. A 116 (1986) 257;
H. Uchimura, H. Fujisaka and M. Inoue, Prog. Theor. Phys. 77 (1987) 1344.
[23] N. Platt, E.A. Spiegel and C. Tresser, Phys. Rev. Lett. 70 (1993) 279.
[24] M. Sano, S. Sato and Y. Sawada, Prog. Theor. Phys. 76 (1986) 945;
R. Benzi, G. Paladin G. Parisi and A. Vulpani, J. Phys. A 18 (1985) 2157.
[25] H. Fujisaka, Prog. Theor. Phys. 70 (1983) 1264;
P. Grassberger, in: Chaos, ed. A.V. Holden (Manchester Univ. Press, Manchester, 1986) pp. 291–311;
P. Grassberger, R. Badii and A. Politi, J. Stat. Phys. 51 (1988) 135.
[26] T. Bohr and D. Rand, Physica D 25 (1987) 387;
T. Bohr and T. Tél, in: Directions in chaos, Vol. 1, ed. Hao Bai-lin (World Scientific, Singapore, 1988) pp. 195–237.
[27] C. Beck and F. Schlögl, Thermodynamics of chaotic systems – An introduction (Cambridge Univ. Press, Cambridge, 1993).
[28] T. Tél, Phys. Rev. A 36 (1987) 2507;
H. Fujisaka and M. Inoue, Prog. Theor. Phys. 78 (1987) 268;
A. Csordás and P. Szépfalusy, Phys. Rev. A 38 (1988) 2582;
M.J. Feigenbaum, J. Stat. Phys. 52 (1988) 527.
[29] K.G. Szabó and T. Tél, Phys. Rev. E 50 (1994) 1070.
[30] Z. Kovács and T. Tél, Phys. Rev. Lett. 64 (1990) 1617; and unpublished.
[31] P. Szépfalusy, T. Tél, A. Csordás and Z. Kovács, Phys. Rev. A 36 (1987) 3525.
[32] M.J. Feigenbaum, I. Procaccia and T. Tél, Phys. Rev. A 39 (1989) 5359.
[33] J.A. Yorke, Y.-C. Lai and C. Grebogi, Nonlinearity 6 (1993) 779.